

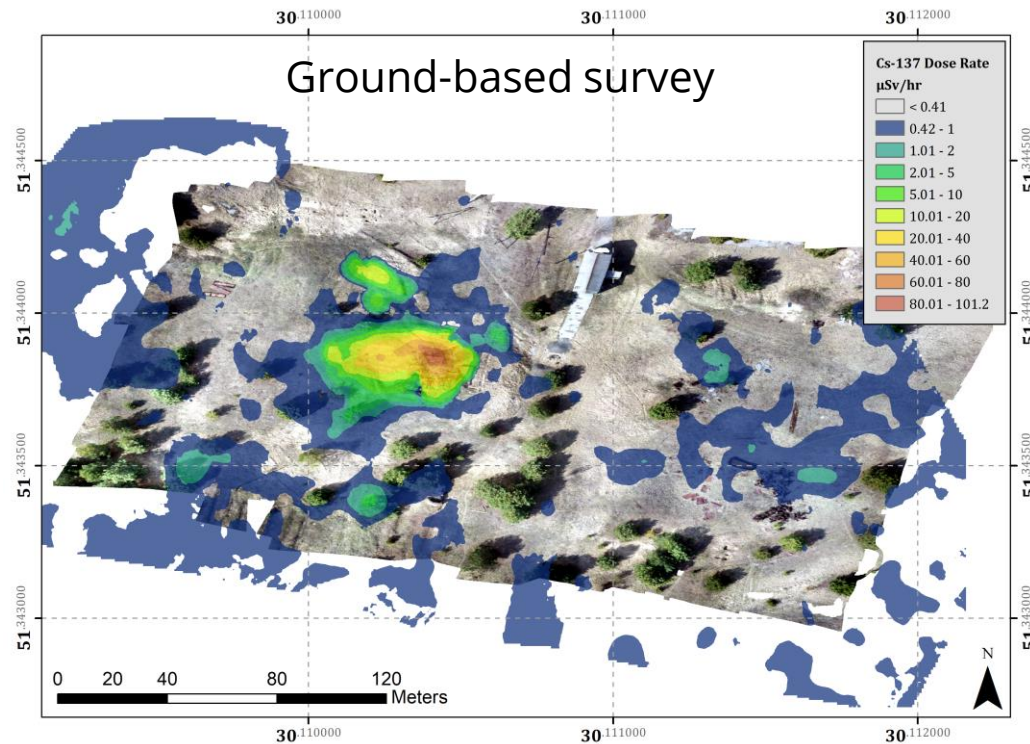
Towards Gamma- Imaging with Limited Pixel Spectrometers

Dr Dean Connor

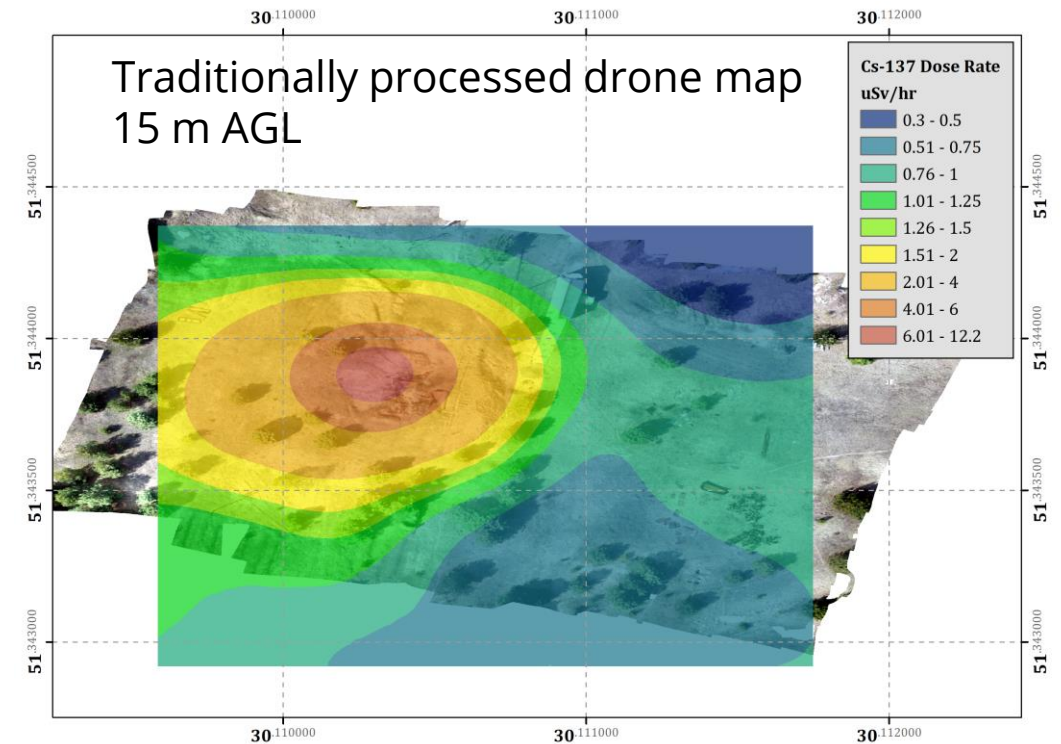
David Megson-Smith, Kieran Wood, Robbie Mackenzie, Euan Connolly, Sam White, Freddie Russell-Pavier, Matthew Ryan-Tucker, Peter Martin, Yannick Verbelen, Thomas Richardson, Nick Smith, and Thomas Scott

Terrain Cognisance in Airborne Gamma Mapping

- 2D mapping taking into account traditional airborne corrections such as assuming a homogenous, infinite distribution within the effective field of view of the detector produce inaccurate maps for heterogeneous hot spots. → See IAEA Techdoc 363 – $E_i(\mu h)$ altitude correction and conversion to activity.
- Accounting for only the vertical distance below the detector is also insufficient for producing accurate maps.

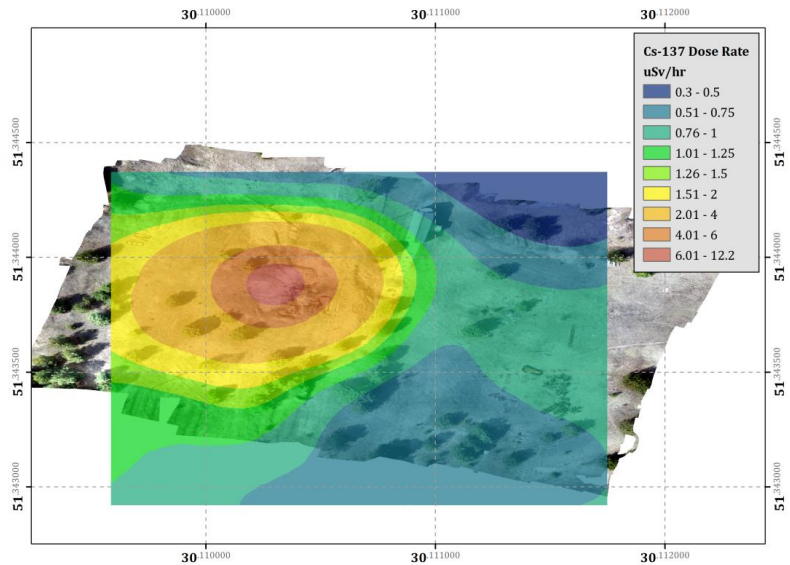
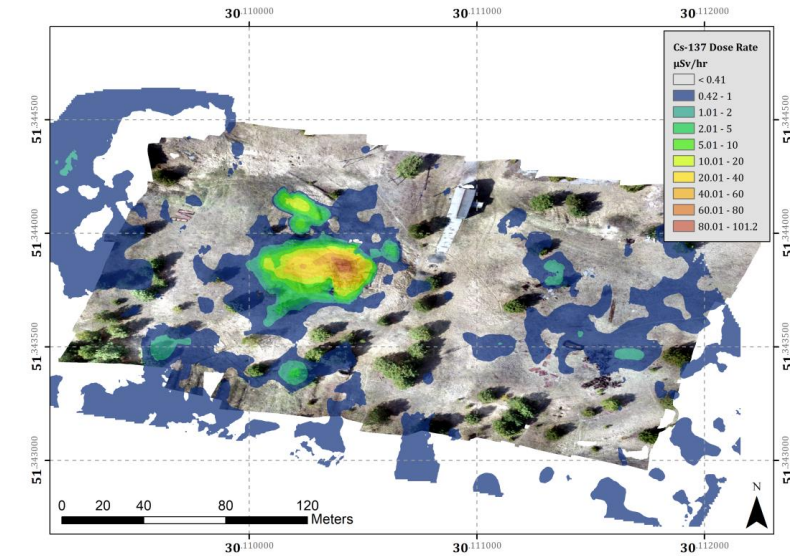


Not protectively marked

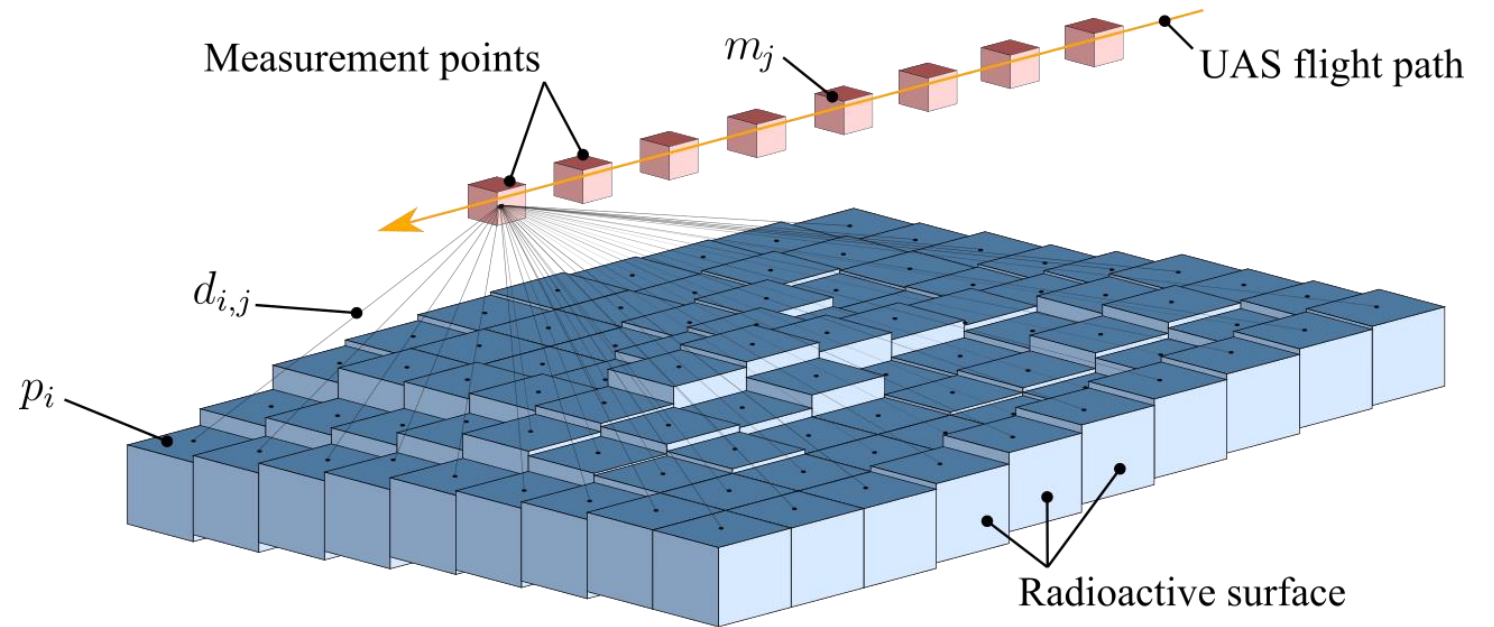


Terrain Cognisance in Airborne Gamma Mapping

- Need to account for the correct distances to all contributing surfaces and the response of the detector in 3D.
- Limited-pixel detectors without imaging capabilities mean that these problems can become complex and poorly conditioned.
- **Requires a 3D map – Photogrammetry or LiDAR**



Not protectively marked



$$p_i = [x_i, y_i, z_i, v_i] \quad m_j = [x_j, y_j, z_j, v_j]$$

Point Cloud Constrained Backprojection (PCCB)

$$\mathbf{S} = \begin{bmatrix} x_1 & y_1 & z_1 & G_1 \\ x_j & y_j & z_j & G_j \\ x_n & y_n & z_n & G_n \end{bmatrix} \quad \mathbf{M} = \begin{bmatrix} x_1 & y_1 & z_1 & p_1 \\ x_i & y_i & z_i & p_i \\ x_n & y_n & z_n & p_n \end{bmatrix}$$

The photopeak intensity (p) within a set of measurements (\mathbf{M}) around a given solution space (\mathbf{S}), is determined by:

$$p_i = \sum_{i=1}^n G_j Y \eta_{ij} \varsigma_{ij} \Delta t + b \Delta t$$

Where:

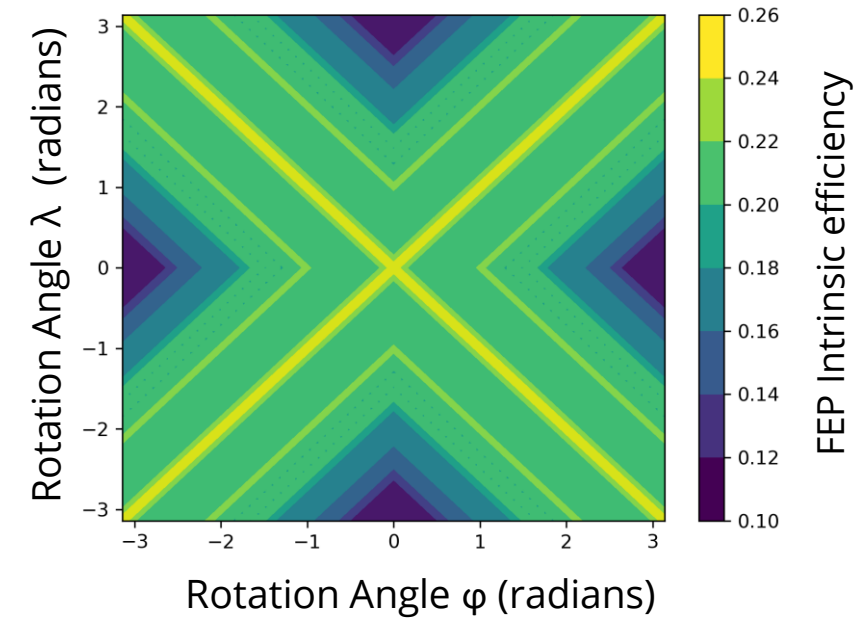
R_{ij} = The distance between point M_i and S_j .

$G_j Y$ = The product of the activity of the gamma emission yield.

η_{ij} = Product of full energy peak (FEP) intrinsic efficiency at incidence angle (λ , φ) and geometrical efficiency encompassing the path distance and presented cross-sectional area of the detector.

ς_{ij} = The attenuation of the gamma rays along the path.

b , Δt = background count rate and measurement time



$$proximity = \sum_{i=1}^n \frac{\Delta t}{4\pi R_{ij}^2}$$

Algebraic Reconstruction Techniques (ART)

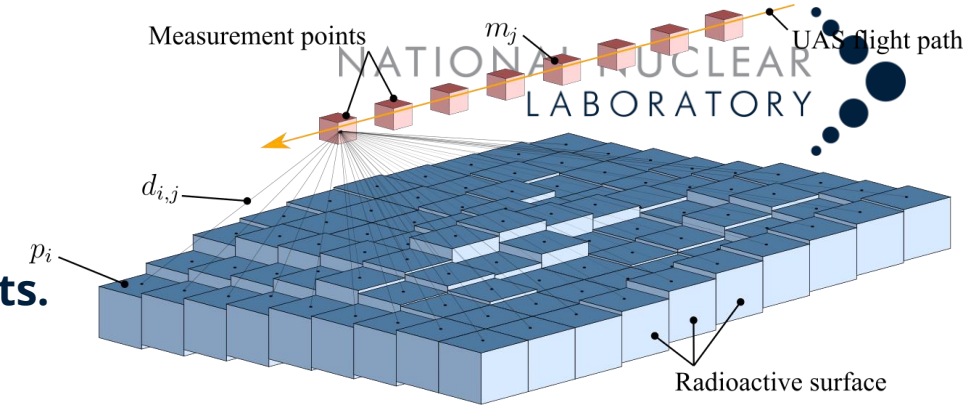
We have a complex linear system that can be described by $\mathbf{Ax} = \mathbf{b}$.

\mathbf{x} = Our solution space. (length of \mathbf{j})

\mathbf{b} = Our measurements. (length of \mathbf{i})

\mathbf{A} = The projection that maps our solution to our measurements.

[Matrix of size ($\mathbf{i} \times \mathbf{j}$)] Individual elements = a_i



$$p_i = [x_i, y_i, z_i, v_i] \quad m_j = [x_j, y_j, z_j, v_j]$$

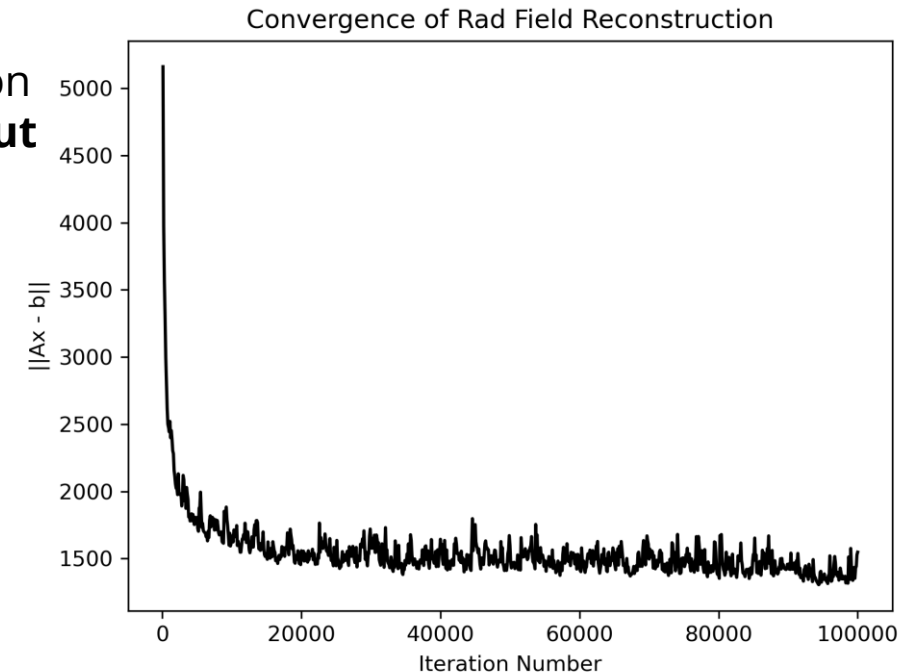
Our results contain an amount of noise and uncertainty and so the true solution can only be really be estimated from our data.

The best fit solution is calculated through performing an iterative, randomized Kaczmarz (rKacz) (S.Kaczmarz, 1937) algorithm combined with an L-normalization optimization, based around minimizing the residual of $\mathbf{Ax} - \mathbf{b}$ for the given input data.

$$x^{k+1} = x^k + \lambda \frac{b_i - a_i x^k}{||a_i||^2} \bar{a}_i$$

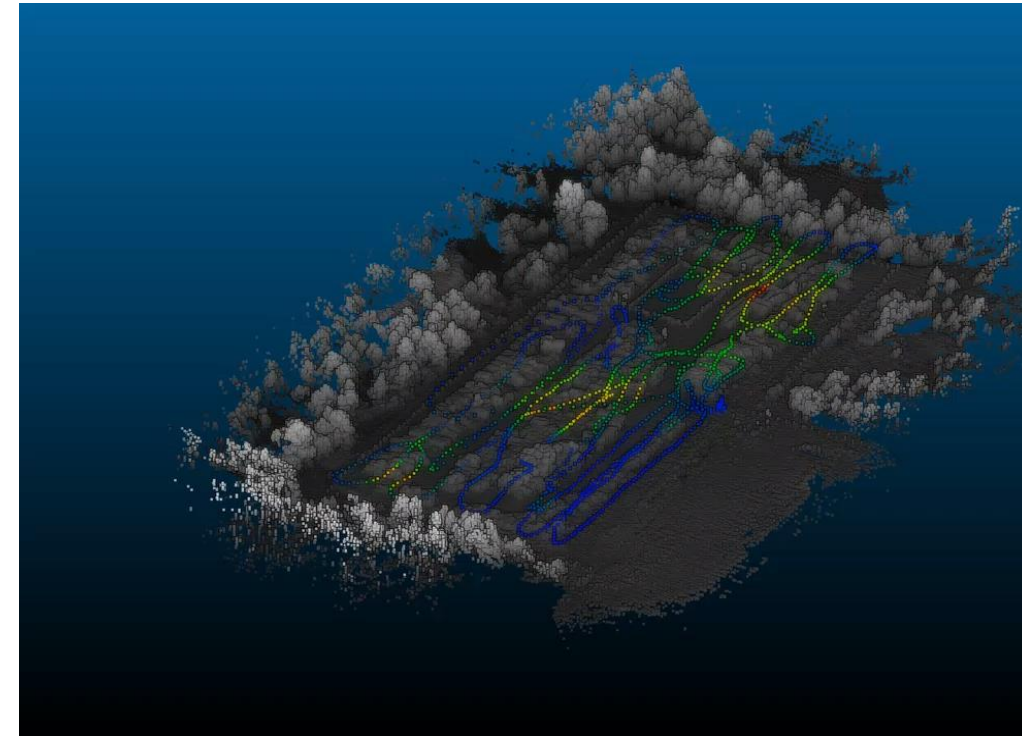
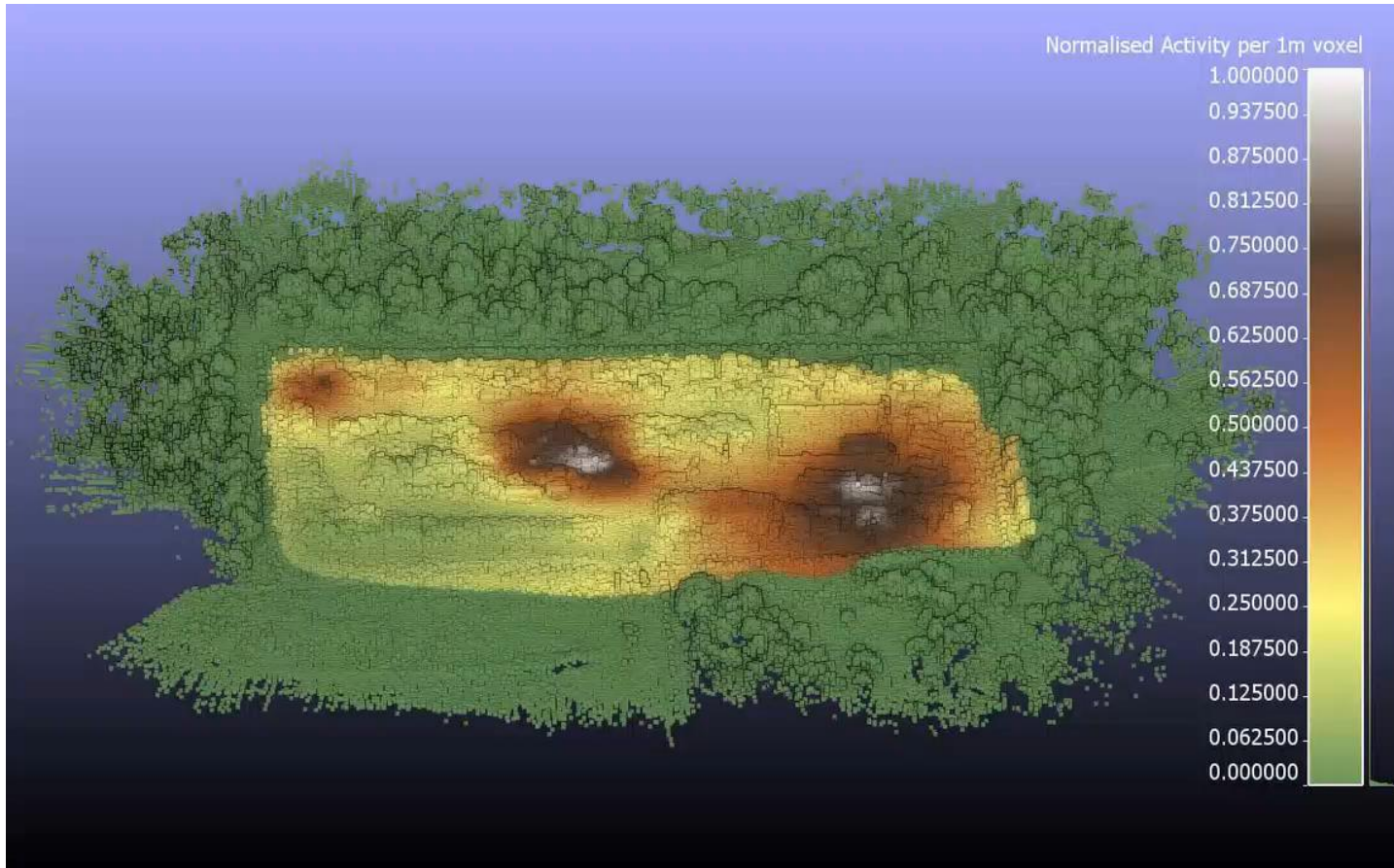
$$x_{bf} = \operatorname{argmin} (||b - Ax||) \quad \text{L}_2 \text{ or L}_1 \text{ norm can be used!}$$

Not protectively marked



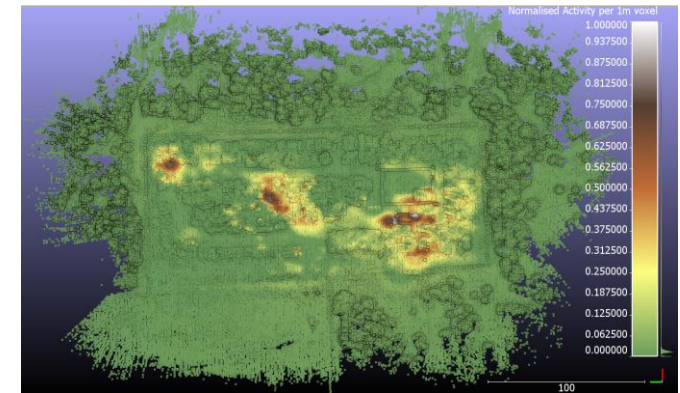
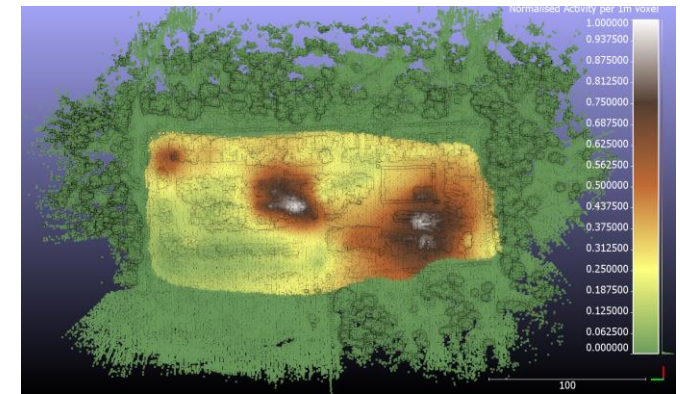
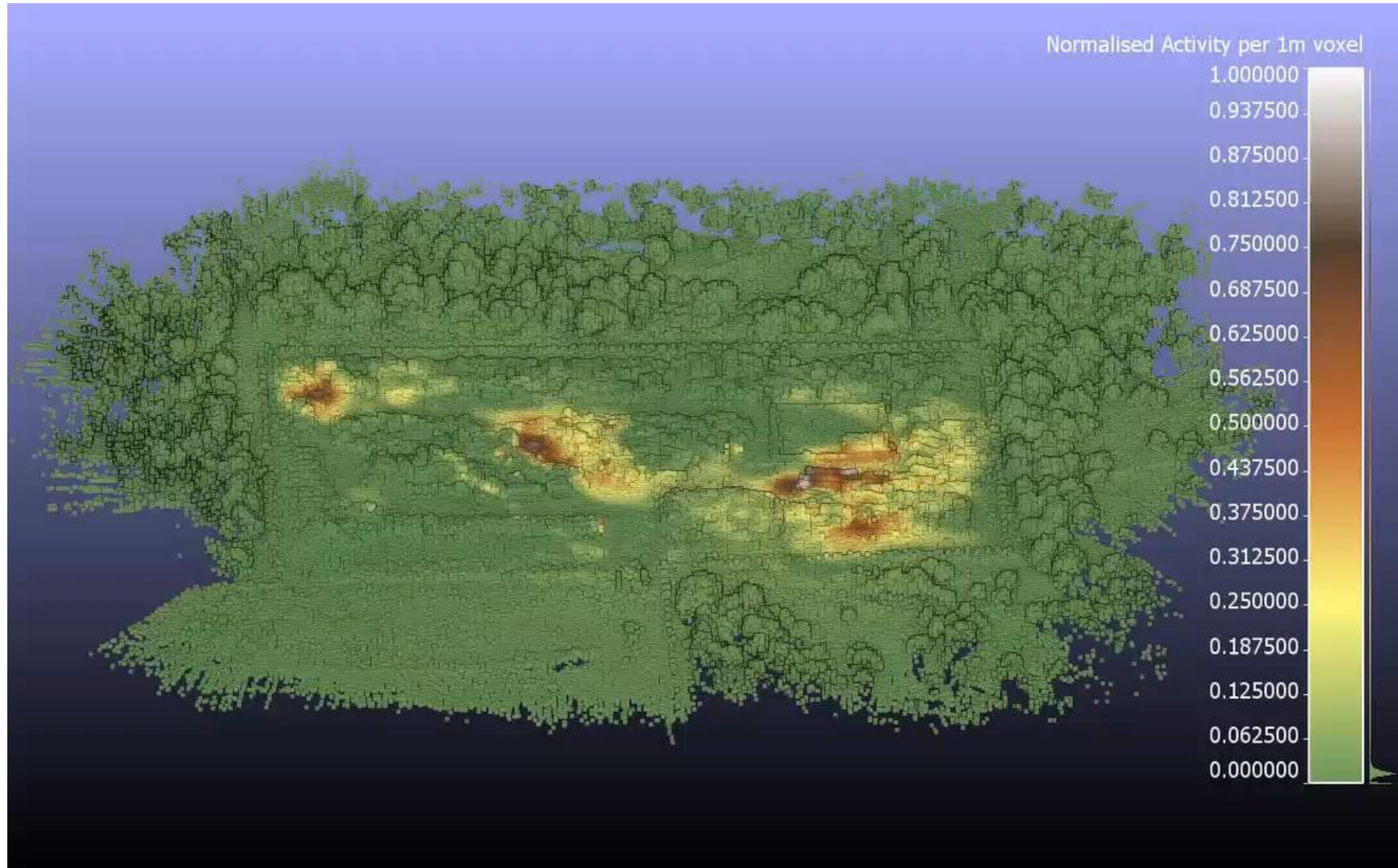
PCCB Example from Chornobyl Exclusion Zone

PCCB applied to data presented to the right.
Specific topographical features relating to hot spots can be identified, better localization, but still significant blurring!



LiDAR point cloud (greyscale) displayed with aerial 662 keV photopeak intensity displayed alongside (blue-red colour scale).

ART (Randomised-Kaczmarz) Example from Chornobyl Exclusion Zone



Note – These two above are not normalized to the same scale!

The ART algorithm effectively reduces the blurring associated with the standard mapping and more accurately reflects the distribution across the site.

Thank you

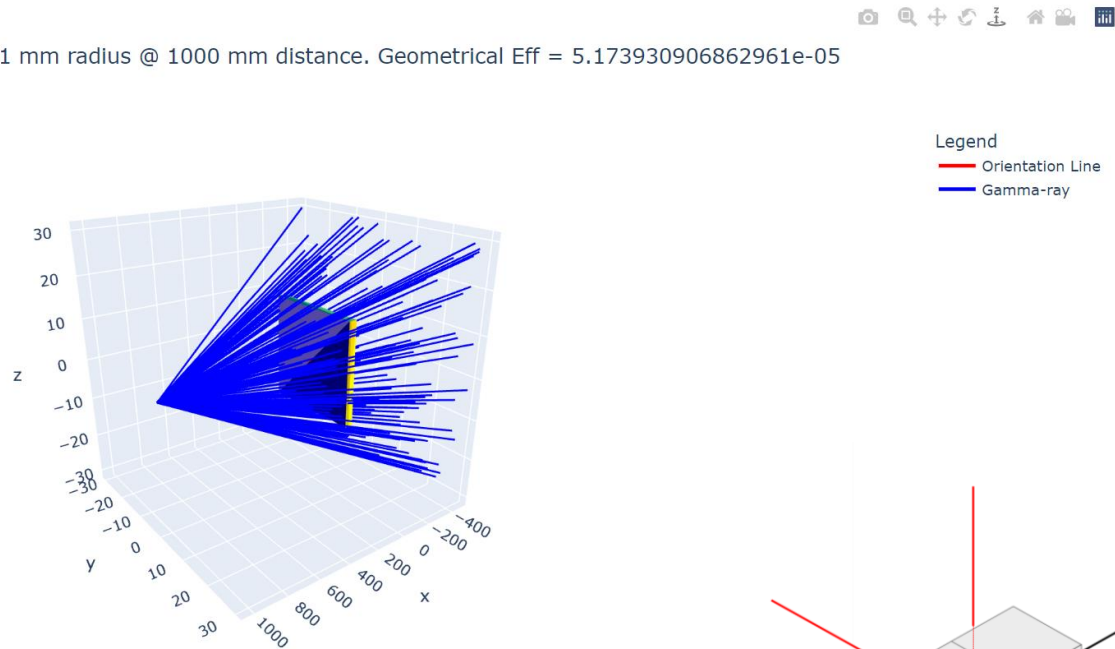
- NNL funding for my Postdoctoral position through the Decontamination and Waste Characterisation R&D fund.
- National Centre for Nuclear Robotics additional funding for my Postdoctoral position.
- NNUF Hot Robotics for access to the equipment used in this work.
- Ukrainian authorities CERWM, SAUEZM and SSE EcoCentre for organising access to the CEZ and supporting our work.

National Nuclear Laboratory
5th Floor, Chadwick House
Warrington Road, Birchwood Park
Warrington WA3 6AE
T. +44 (0) 1925 933 744
E. customers@uknnl.com
www.nnl.co.uk

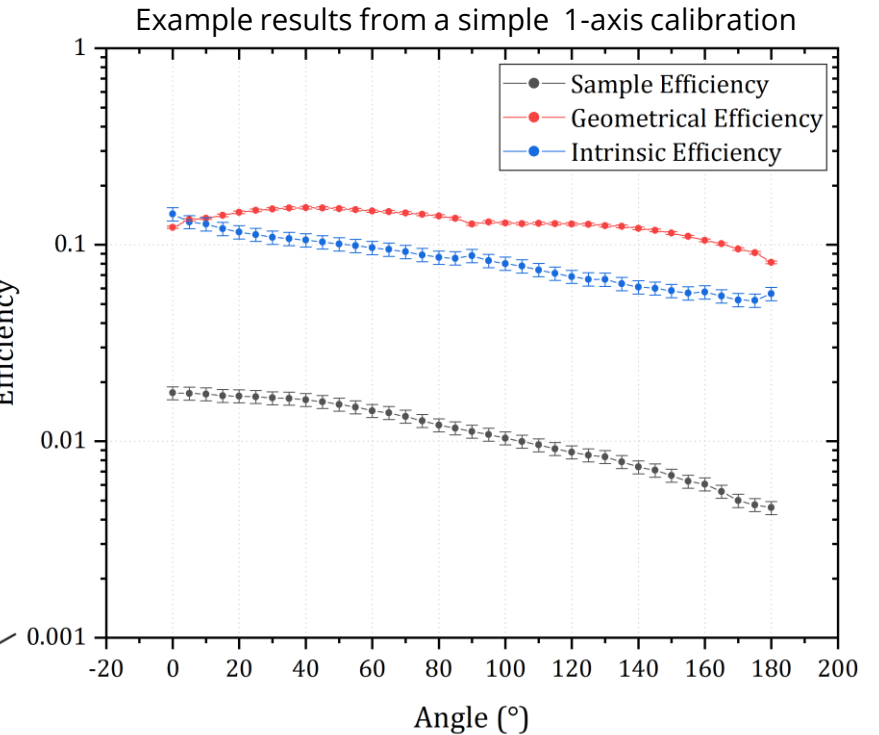
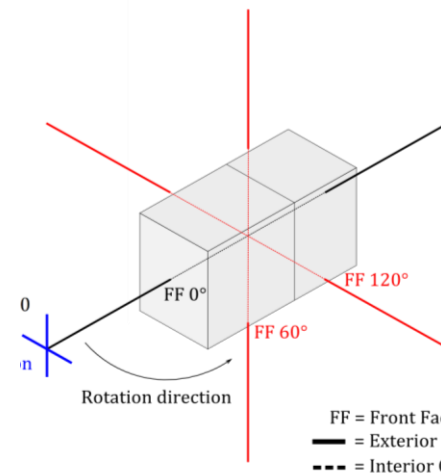
Supplementary Slide – Calibration of Responses

- Combination of empirical experiments using calibrated point sources with in-house Monte (MC) Carlo modelling to understand geometrical considerations.

Detector Sim: sphere source = 0.1 mm radius @ 1000 mm distance. Geometrical Eff = 5.173930906862961e-05



MC modelling
software built in
Python.

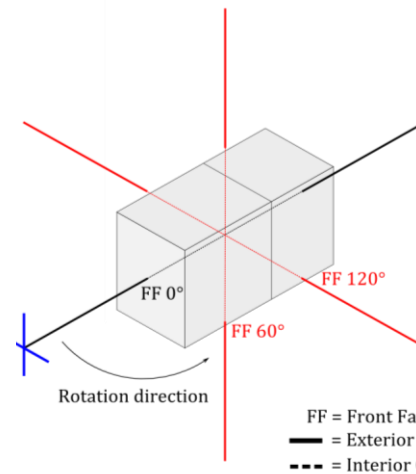
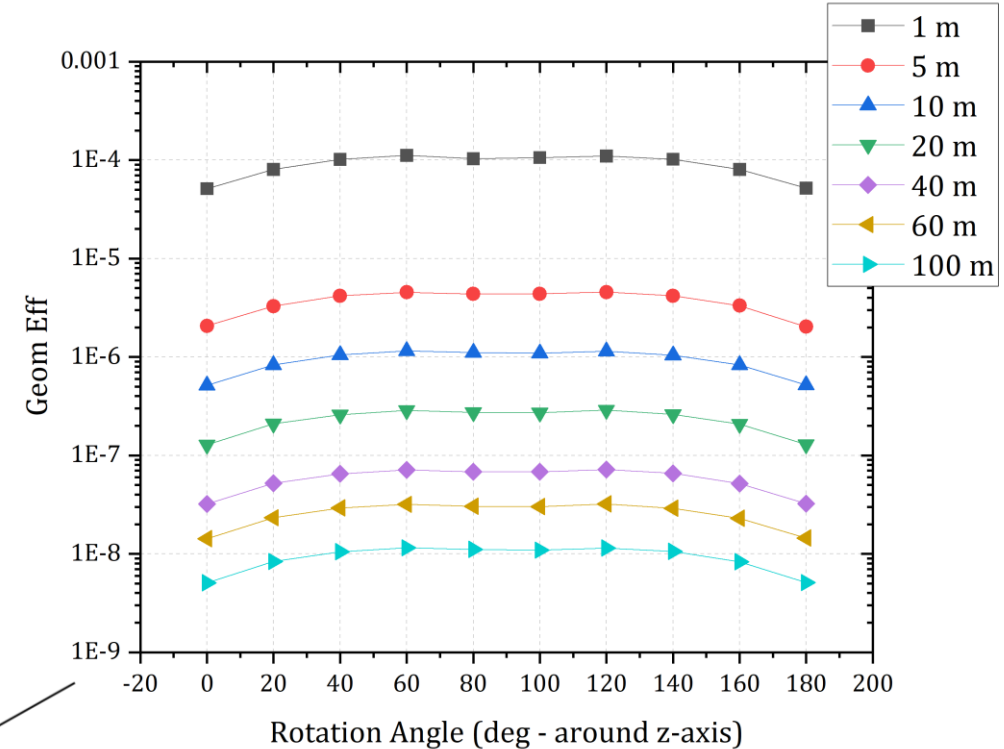
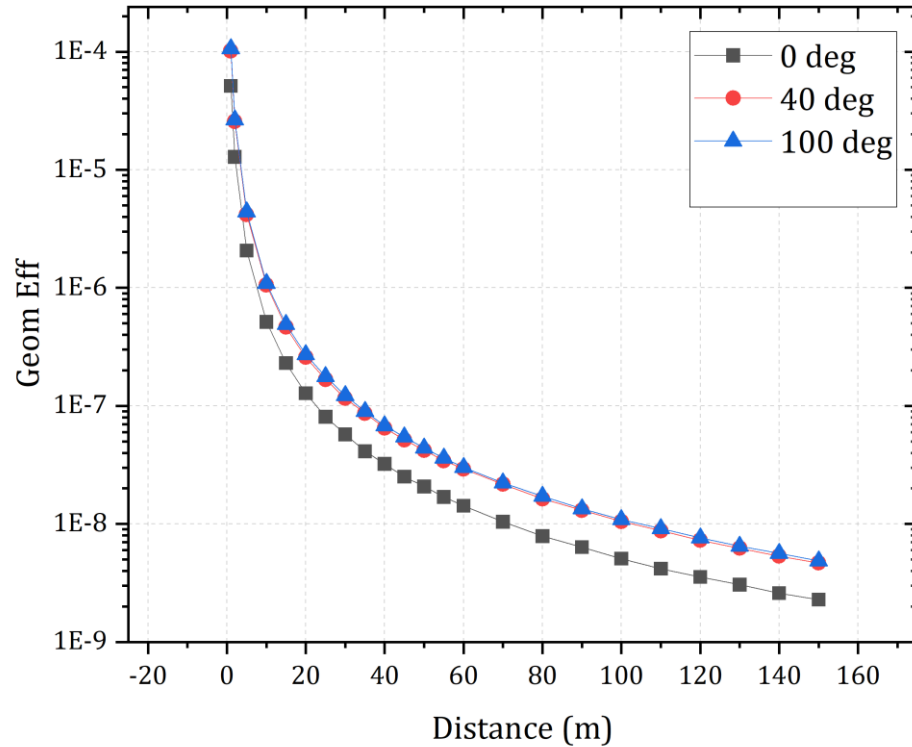


Rotation around the z-axis.
x-axis points out of the front face of the cuboid-shaped detector.

Supplementary Slide – Calibration of Responses

- Combination of empirical experiments using calibrated point sources with in-house Monte (MC) Carlo modelling to understand geometrical considerations.

Example results from a simple 1-axis calibration



Rotation around the z-axis.
x-axis points out of the front face of the cuboid-shaped detector.